Observation of superconductivity accompanying the pressure-induced structural phase transition in LaSb

Min Zhang,[1] Xiangqi Wang,[1] Azizur Rahman,[1] Rucheng Dai,[2] Zhongping Wang,[2] and Zengming Zhang[1,2,*]

[1]*CAS Key Laboratory of Strongly Coupled Quantum Matter Physics, and Department of Physics, University of Science and Technology of China, Hefei, Anhui 230026, China*

[2]*Center of Physical Experiments, University of Science and Technology of China, Hefei 230026, China*

(Received 30 November 2019; accepted 3 February 2020; published 25 February 2020)

LaSb has attracted intense interest due to the recent discovery of its extreme magnetoresistance (XMR) and controversial topology states. Motivated by the existing structural phase transition and the possible topological phase transition, the electrical transport properties of a LaSb single crystal under pressure up to 35 GPa were investigated. Superconductivity appears at 10.8 GPa, and the critical temperature (T_c) rapidly reaches a maximum of 5.3 K at 13.7 GPa and then linearly decreases with further loading pressure, which can be represented by a typical dome-shaped superconducting phase diagram. The superconductivity is believed to originate from the significant increase of the density of states near the Fermi level [$N(E_F)$], which is induced by the volume collapse due to the structural transition from cubic to tetragonal at approximately 10.8 GPa. This result has inspired systematic studies of the LnX (Ln = lanthanide and X = P, As, Sb, Bi) family under high pressure, especially superconductivity investigations.

DOI: 10.1103/PhysRevB.101.064106

I. INTRODUCTION

Rare-earth-metal monopnictides LnX (Ln = lanthanide and X = P, As, Sb, Bi) have been studied for several decades as examples of typical materials possessing unoccupied 4f states [1–3]. One of their essential properties is the pressure-induced structural phase transition. Recently, interest has increased as a result of the extreme magnetoresistance (XMR) in LaSb [4,5], and LnX was added to the family of XMR materials [6–10]. LnX supports an ideal platform with which to study the underlying physics of the XMR phenomenon as well as the relevant electronic band topology and superconductivity [10–13].

The structural and electronic properties of LnX under high pressure have been intensively studied both theoretically [3,14] and experimentally [15]. LaX crystallizes in a cubic structure of NaCl type ($B1$ phase) at ambient conditions. Most members undergo a structural phase transition to the primitive tetragonal structure (PT phase) of distorted CsCl type under high pressure, accompanying a large volume collapse of approximately 10%. Theoretical calculations predicted that LaSb transforms from $B1$ to PT in the range 6.9–11 GPa [16,17]. The pressure-volume relationship extracted from the synchrotron x-ray diffraction pattern revealed that the phase transition occurs at 11 GPa [18]. In addition, Guo *et al.* predicted a topological phase transition at 3–4 GPa without breaking any symmetry [19]. However, the electrical transport properties under high pressure have not been reported in LaSb. In addition, analogous studies are very rare for the entire family. On the other hand, pressure can dramatically change the physical properties in different ways [20–23]. It is therefore highly desirable to carry out a thorough study of the intrinsic electrical transport properties of LaSb under high pressure.

In this study, the temperature-dependent electrical resistance and magnetoresistance (MR) of LaSb under high pressure up to 35 GPa are reported. Superconductivity emerges with the formation of PT phase of LaSb above 10.8 GPa, and the upper critical magnetic field H_{c2} for 13.7 GPa is obtained. Implied by the pressure coefficients variations of transport parameters, the coexistence of $B1$ and PT phases is proposed in the range 10.8–13.7 GPa.

II. METHODS

LaSb single crystals were grown by the stannum flux method. A stoichiometric ratio of La:Sb:Sn = 1 : 1 : 20 was mixed and placed in an alumina crucible before being sealed in an evacuated quartz tube. The quartz tube was heated to 1000 °C and slowly cooled to 700 °C at a rate of 2 °C/h, and crystals were finally decanted with centrifugation. Single-crystal samples were obtained with a typical cubic size of 1.5 mm. The structure of the crystals was analyzed by x-ray diffraction (XRD) using a Rigaku diffractometer with Cu Kα radiation. Figure 1 shows the XRD pattern, the obvious (00n) peaks indicating the pure phase crystallization of the samples. A diamond anvil cell (DAC) was used as the high-pressure generator, and pressures were determined from the ruby fluorescence line shift [24]. KBr was used as the pressure-transmitting medium. A sample sheet with a typical thickness of 10 μm was thinned from the cubic bulk and then configured with four platinum electrical probes [25]. The electrical transport measurements were performed

*Corresponding author: zzm@ustc.edu.cn

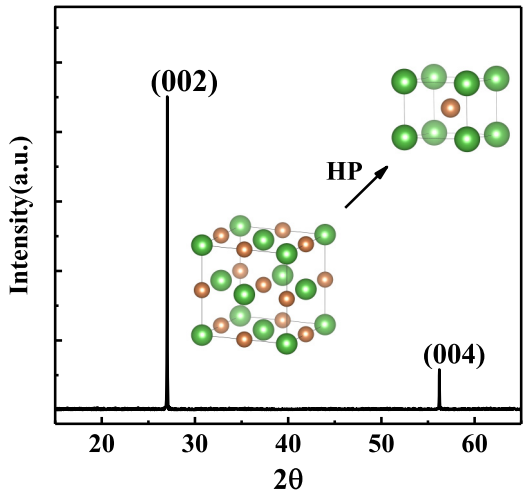

FIG. 1. X-ray diffraction pattern of NaCl type structure of LaSb samples. Strong (00n) peaks can be clearly seen. Lower-middle and upper-right insets correspond to crystal structures for NaCl type (B1 phase) and high-pressure distorted CsCl type (PT phase) of LaSb, respectively.

using a commercial physical property measurement system (DynaCool, Quantum Design).

III. RESULTS AND DISCUSSION

Figure 2 shows the temperature-dependent electrical resistance under high pressure. As shown in Fig. 2(a), the lower pressure data exhibit typical metallic behavior with a residual resistivity ratio (RRR) approximately 10 (RRR is defined as the ratio of the resistivity of a material at room temperature and at 0 K). Up to 10.8 GPa in Fig. 2(b), a sharp drop in resistance appears near 5.1 K, which signifies the occurrence of superconductivity. Upon further compression, the resistance decreases with pressure at low temperature and drops to zero when it reaches 13.7 GPa, indicating the completion of the superconducting transition. This is attributed to the coexistence of two structural phases (described below). The superconducting transition temperature region is characterized by the transition width (from 10% to 90% of the normal-state resistance) of 0.4 K, indicating the good homogeneity of the superconducting phase. Above 13.7 GPa, as shown in Fig. 2(c), the superconducting transition temperature starts to decrease with increasing pressure. Here, the critical temperature (T_c) is defined as the temperature at which the resistance drops to 90% of the normal-state resistance. In summary, the superconductivity sets in at 10.8 GPa, and T_c increases slightly to reach a maximum of 5.3 K at 13.7 GPa and then decreases gradually, which can be shown by a typical superconducting dome phase diagram. Compared with the previous report of the $B1$-PT phase transition at 11 GPa [18], the pressure-induced superconductivity is attributed to the structural phase transition. Notably, in contrast to the isostructural compound LaBi [26], superconductivity was not observed in the $B1$ phase of LaSb under high pressure. Since most elements of lanthanide and pnictogen are superconducting at ambient or at high pressure [27–30], it is recommended that the effects

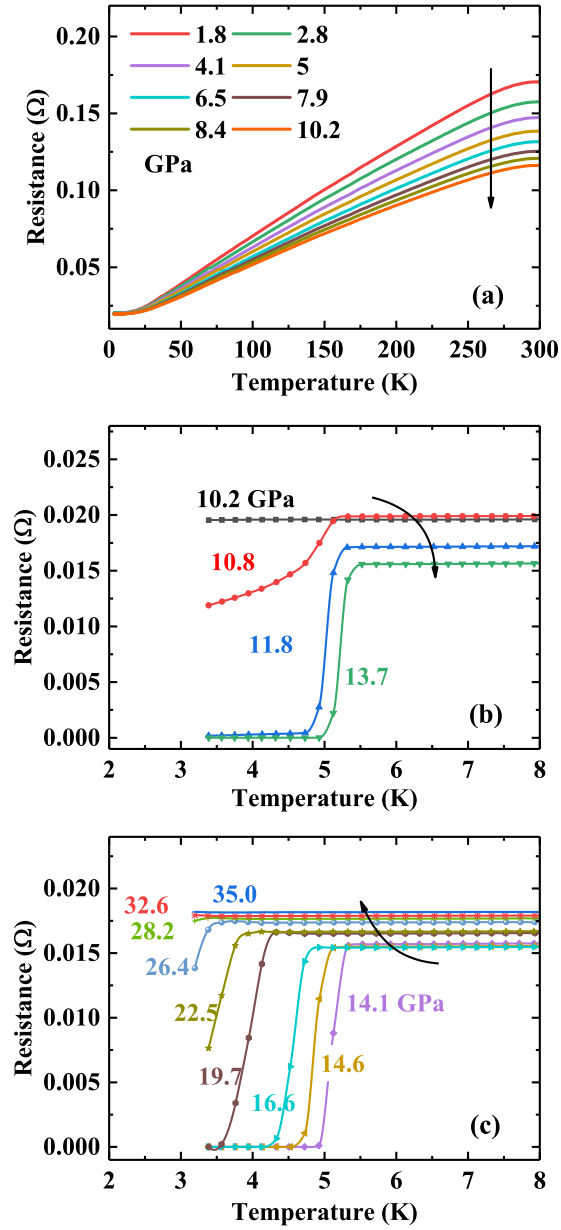

FIG. 2. Electrical resistance of LaSb single crystals as a function of temperature at various applied pressures.

of the elements and defects on superconductivity behavior receive more careful investigation in the future.

The presence of pressure-induced superconductivity in LaSb was further corroborated by the resistance measurements under external magnetic fields. Figure 3(a) shows the temperature dependence of resistance with applied magnetic fields vertical to the current at 13.7 GPa. Resistance drops are gradually induced to lower temperature with increasing field, which is typical for a bulk superconducting transition. It can be seen that the onset point of transition shifts slowly with the magnetic field, but the zero resistance point shifts more quickly to lower temperature. This is understandable since the latter is determined by the weak links between the grains as well as the vortex flow behavior, while the former is controlled by the upper critical field (H_{c2}) of the individual

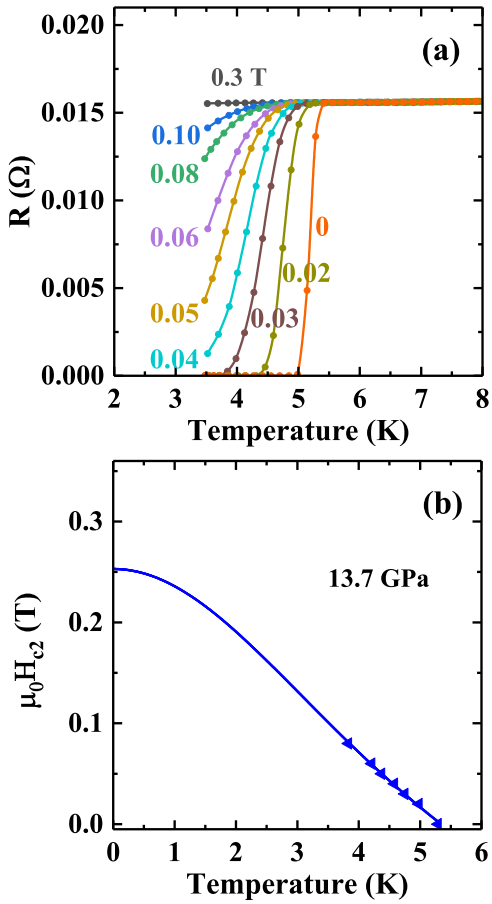

FIG. 3. Upper critical field analysis of LaSb superconductor. (a) Temperature dependence of resistance with applied field up to 0.3 T at 13.7 GPa. (b) $H_{c2} - T_c$ phase diagram at 13.7 GPa. T_c is determined as the 90% drop of normal-state resistance. Solid line represents fitting by Eq. (1) and $H_{c2}(0)$ is estimated to be 0.25 T.

grains [31]. Figure 3(b) displays H_{c2} as a function of T_c; the zero-temperature H_{c2} [$H_{c2}(0)$] is estimated to be 0.25 T at 13.7 GPa by using the extended Ginzburg-Landau formula [32]:

$$H_{c2}(T) = H_{c2}(0)\frac{1-(T/T_c)^2}{1+(T/T_c)^2}. \quad (1)$$

$H_{c2}(0)$ is far below the Bardeen-Cooper-Schrieffer (BCS) weak-coupling Pauli limit of 1.84 $T_c = 9.7$ T for $T_c = 5.3$ K [33,34].

MR evolutions under high pressure are now discussed. Large-MR materials have received great attention not only because of their promising applications as magnetic storage device, spin valves, etc., but also owing to their rich physical information, e.g., carriers, dynamic scattering, and electronic and crystal structure. MR is defined as MR = $[R(H) - R(0)]/R(0)$, which expresses the electrical resistance change ratio with applied magnetic field. Here, $R(0)$ is the normal-state resistance at zero field, which was extracted from the parabolic curve fitting to our high-field data. Figure 4(a) shows MR as a function of magnetic field measured at $T =$ 3.5 K under high pressure. As the MR magnitude of LaSb is extremely sensitive to the RRR, a quadratic dependence

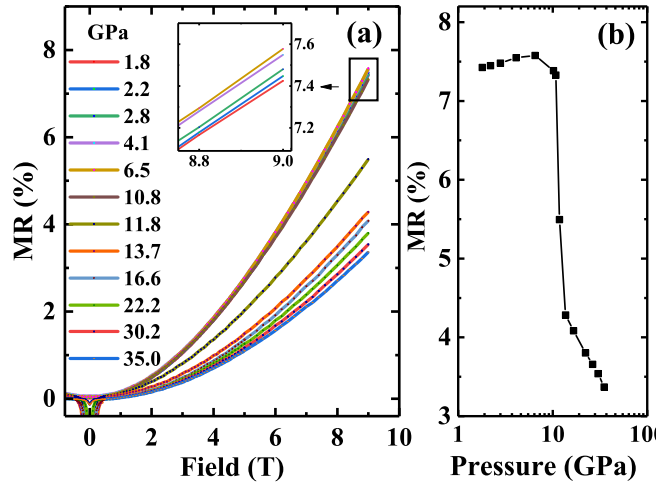

FIG. 4. (a) Magnetic field dependence of MR at $T = 3.5$ K under high pressure up to 35 GPa. Inset shows the enlarged image for the region of lower pressure and high field. (b) Pressure-dependent MR amplitude at $H = 9$ T and $T = 3.5$ K.

equation of MR $= 10^{-3}$ RRR^2 has been reported by Tafti *et al.* [4,6]. The XMR phenomena were not observed in the current work due to the small RRR, which probably is introduced by the crystallographic defect; even so, the pure $B1$ phase of LaSb single crystal is confirmed through the XRD pattern as shown in Fig. 1. Figure 4(b) shows a drastic suppression of MR near the structural phase transition region; meanwhile, a pressure coefficient inflection appears near 6 GPa, which can be seen in the inset of Fig. 5 as well. The mean mobility of carriers, μ_m, should exhibit the coincident trend versus pressure as result of the relationship of MR $= \mu_m^2 H^2$ [35].

Figure 5 summarizes the temperature-pressure phase diagram. In general, the pressure-driven superconductivity is often accompanied by a structural phase transition, most of which lead to anomalies in normal-state resistivity [36–40]. In Summerfeld's modes, electrical resistance is written as $R = 1/n(E_F)e\mu_m$. Here, $n(E_F)$ and μ_m represent the carrier density near the Fermi energy and the mean mobility of carriers, respectively [41]. Dominated by both of these, the electrical resistance carries information that is critically important to understanding the high-pressure behavior of materials.

In the $B1$ phase, the residual resistance R_{10K} shows a slope change after 6 GPa, and then a more gentle attenuation is clearly visible. This is comparable with the MR variation in the same range as shown in the inset of Fig. 5. The inflection point is obtained as 5.5 GPa from linear fitting of R_{10K} data. Guo *et al.* theoretically predicted the pressure-induced topological phase transition at approximately 3–4 GPa [19]. It is surmised that the pressure coefficient changes in both residual resistance and MR are possibly related to the topological phase transition. Similar slope changes associated with the electronic topological transition have been identified in numerous materials, e.g., $AuIn_2$ [42], BP [43], and BiTeBr [44]. Further confirmation is needed, however, and the relationship between XMR effect and pressure merits further study.

When LaSb starts to transform into the PT phase, the most striking finding is that R_{10K} shows an abrupt drop in the range

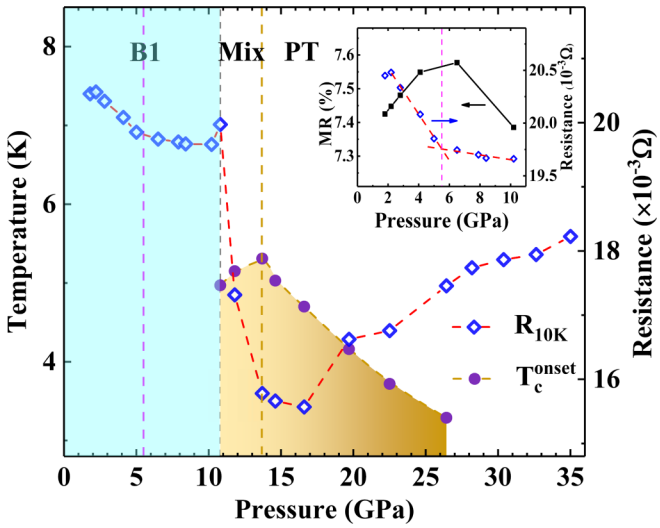

FIG. 5. Temperature vs pressure phase diagram. Left-hand axis denotes T_c and right-hand axis corresponds to residual resistance R_{10K}. Superconductivity appears at 10.8 GPa, where the structural transition takes place as denoted by the gray dashed line. Pink and yellow dashed lines near 5 and 14 GPa, respectively, mark the boundaries where the possible topological phase transition occurs and the $B1$-PT transformation finishes, respectively. Inset shows a magnification of residual resistance R_{10K} and MR in the region of lower pressure. Red dashed lines are linear fitting curves in the ranges 1.8–5.0 and 6.5–10.2 GPa, respectively, from which the inflection point is extracted as 5.5 GPa.

10.8–13.7 GPa, after which an upshift appears. From previous reports, the structural phase transition in LaSb was accompanied by a large volume collapse of 10.1% [18]; simultaneously, *ab initio* calculations indicated that the density of states near the Fermi level [$N(E_F)$] exhibits a significant increase from 3 to 10–15 states/Ry cell [16,17]. Thus, the pressure-induced $N(E_F)$ increase should be the origin of the sharp decrease of the residual resistance and, correspondingly, the occurrence of superconductivity [45]. Meanwhile, the broad range of the R_{10K} drop could be related to the coexistence of $B1$ and PT phases, while similar mixed phases were observed in other isostructural compounds [46]. Therefore, the initial increase of T_c with compression probably results from the increasing of the superconducting phase proportion. Upon further compression, T_c shows a linear decrease. The negative pressure coefficient is commonly attributed to the volume dependence of $N(E_F)$ and of the effective interaction between the electrons mediated by the electron-phonon coupling [47], which is typical in metal element superconductivity [48]. As implied by the inflected increase in R_{10K}, the linear decrease in T_c can be explained by the shrinking of $N(E_F)$ with increasing pressure.

IV. SUMMARY

In summary, the electrical transport measurements conducted in this work reveal superconductivity rooted in the high-pressure PT phase of LaSb. The $T_c - P$ phase diagram is obtained, and, corresponding to the transition from the $B1$ to PT phase, an abrupt drop appears both in residual resistance and MR between 10.8 and 13.7 GPa, where a typical superconducting dome starts to form. Based on the previous electronic band calculations, the superconductivity is attributed to the significant increase of $N(E_F)$ due to structural instability. Conclusively, one mixed phase containing $B1$ and PT phases is proposed in the range 10.8–13.7 GPa, leading to the initial increase of T_c, after which a typical linear decrease of T_c is observed. In the $B1$ phase, possible signals of the topological phase transition near 5.5 GPa are also found, but further confirmation is needed. In light of the common structural phase transition occurring in LnX, more superconducting compounds and related physics can be expected in the entire LaX family. It should be noted that the superconductivity identified in the $B1$ phase of LaBi was not observed in LaSb, and the distinct transport properties reported here indicate promising prospects for further investigation of the LaX family, in particular the elements' effects and the high-pressure behaviors.

ACKNOWLEDGMENTS

This work was financially supported by the Science Challenge Project (TZ2016001).

[1] W. Zachariasen and F. Ellinger, Acta Crystallogr. Sect. A **33**, 155 (1977).
[2] A. Hasegawa, J. Phys. C **13**, 6147 (1980).
[3] A. Hasegawa, J. Phys. Soc. Jpn. **54**, 677 (1985).
[4] F. F. Tafti, Q. D. Gibson, S. K. Kushwaha, N. Haldolaarachchige, and R. J. Cava, Nat. Phys. **12**, 272 (2015).
[5] L. K. Zeng, R. Lou, D. S. Wu, Q. N. Xu, P. J. Guo, L. Y. Kong, Y. G. Zhong, J. Z. Ma, B. B. Fu, P. Richard, P. Wang, G. T. Liu, L. Lu, Y. B. Huang, C. Fang *et al.*, Phys. Rev. Lett. **117**, 127204 (2016).
[6] F. Fallah Tafti, Q. Gibson, S. Kushwaha, J. W. Krizan, N. Haldolaarachchige, and R. J. Cava, Proc. Nat. Acad. Sci. U.S.A. **113**, E3475 (2016).
[7] S. Sun, Q. Wang, P. Guo, K. Liu, and H. Lei, New J. Phys. **18**, 082002 (2016).
[8] J. He, C. Zhang, N. J. Ghimire, T. Liang, C. Jia, J. Jiang, S. Tang, S. Chen, Y. He, S. K. Mo, C. C. Hwang, M. Hashimoto, D. H. Lu, B. Moritz, T. P. Devereaux *et al.*, Phys. Rev. Lett. **117**, 267201 (2016).
[9] N. Wakeham, E. D. Bauer, M. Neupane, and F. Ronning, Phys. Rev. B **93**, 205152 (2016).
[10] Z. M. Wu, Y. R. Ruan, F. Tang, L. Zhang, Y. Fang, J. M. Zhang, Z. D. Han, R. J. Tang, B. Qian, and X. F. Jiang, New J. Phys. **21**, 093063 (2019).
[11] R. Lou, B. B. Fu, Q. N. Xu, P.-J. Guo, L.-Y. Kong, L.-K. Zeng, J.-Z. Ma, P. Richard, C. Fang, Y.-B. Huang, S.-S. Sun, Q. Wang, L. Wang, Y.-G. Shi, H. C. Lei *et al.*, Phys. Rev. B **95**, 115140 (2017).
[12] W. J. Ban, D. S. Wu, C. C. Le, J. P. Hu, J. L. Luo, and H. Xiao, Phys. Rev. B **100**, 115133 (2019).

[13] S. Khalid, F. P. Sabino, and A. Janotti, Phys. Rev. B **98**, 220102(R) (2018).
[14] Y. Kaneta, O. Sakai, and T. Kasuya, Phys. B (Amsterdam, Neth.) **186–188**, 156 (1993).
[15] R. Settai, T. Goto, S. Sakatsume, Y. S. Kwon, T. Suzuki, and T. Kasuya, Phys. B (Amsterdam, Neth.) **186–188**, 176 (1993).
[16] G. Vaitheeswaran, V. Kanchana, and M. Rajagopalan, Phys. B (Amsterdam, Neth.) **315**, 64 (2002).
[17] Z. Charifi, A. H. Reshak, and H. Baaziz, Solid State Commun. **148**, 139 (2008).
[18] J. M. Leger, D. Ravot, and J. Rossat-Mignod, J. Phys. C **17**, 4935 (1984).
[19] P.-J. Guo, H.-C. Yang, K. Liu, and Z.-Y. Lu, Phys. Rev. B **96**, 081112(R) (2017).
[20] H. Q. Yuan, F. M. Grosche, M. Deppe, C. Geibel, G. Sparn, and F. Steglich, Science **302**, 2104 (2003).
[21] S. Gabani, E. Bauer, S. Berger, K. Flachbart, Y. Paderno, C. Paul, V. Pavlák, and N. Shitsevalova, Phys. Rev. B **67**, 172406 (2003).
[22] X. Wang, Z. Li, M. Zhang, T. Hou, J. Zhao, L. Li, A. Rahman, Z. Xu, J. Gong, Z. Chi, R. Dai, Z. Wang, Z. Qiao, and Z. Zhang, Phys. Rev. B **100**, 014407 (2019).
[23] M. Zhang, X. Wang, A. Rahman, Q. Zeng, D. Huang, R. Dai, Z. Wang, and Z. Zhang, Appl. Phys. Lett. **112**, 041907 (2018).
[24] H. K. Mao, J. A. Xu, and P. M. Bell, J. Geophys. Res. **91**, 4673 (1986).
[25] H. K. Mao and P. M. Bell, Rev. Sci. Instr. **52**, 615 (1981).
[26] F. F. Tafti, M. S. Torikachvili, R. L. Stillwell, B. Baer, E. Stavrou, S. T. Weir, Y. K. Vohra, H. Y. Yang, E. F. McDonnell, S. K. Kushwaha, Q. D. Gibson, R. J. Cava, and J. R. Jeffries, Phys. Rev. B **95**, 014507 (2017).
[27] J. Wittig, J. Phys. Chem. Solids **30**, 1407 (1969).
[28] M. B. Maple, J. Wittig, and K. S. Kim, Phys. Rev. Lett. **23**, 1375 (1969).
[29] M. A. Il'Ina, E. S. Itskevich, and E. M. Dizhur, Sov. Phys. JETP **34**, 1263 (1972).
[30] N. Lotter and J. Wittig, EPL **6**, 659 (1988).
[31] X. Zhu, H. Yang, L. Fang, G. Mu, and H.-H. Wen, Superconductor Sci. Technol. **21**, 105001 (2008).
[32] J. A. Woollam, R. B. Somoano, and P. O'Connor, Phys. Rev. Lett. **32**, 712 (1974).
[33] A. M. Clogston, Phys. Rev. Lett. **9**, 266 (1962).
[34] C. K. Poole, H. A. Farach, and R. J. Creswick, *Handbook of Superconductivity* (Elsevier, Amsterdam, 1999).
[35] P.-J. Guo, H.-C. Yang, B.-J. Zhang, K. Liu, and Z.-Y. Lu, Phys. Rev. B **93**, 235142 (2016).
[36] Y. Liu, Y. J. Long, L. X. Zhao, S. M. Nie, S. J. Zhang, Y. X. Weng, M. L. Jin, W. M. Li, Q. Q. Liu, Y. W. Long, R. C. Yu, C. Z. Gu, F. Sun, W. G. Yang, H. K. Mao *et al.*, Sci. Rep. **7**, 44367 (2017).
[37] Y. Qi, W. Shi, P. G. Naumov, N. Kumar, R. Sankar, W. Schnelle, C. Shekhar, F.-C. Chou, C. Felser, B. Yan, and S. A. Medvedev, Adv. Mater. **29**, 1605965 (2017).
[38] M. L. Jin, F. Sun, L. Y. Xing, S. J. Zhang, S. M. Feng, P. P. Kong, W. M. Li, X. C. Wang, J. L. Zhu, Y. W. Long, H. Y. Bai, C. Z. Gu, R. C. Yu, W. G. Yang, G. Y. Shen *et al.*, Sci. Rep. **7**, 39699 (2017).
[39] Y. Zhou, J. Wu, W. Ning, N. Li, Y. Du, X. Chen, R. Zhang, Z. Chi, X. Wang, X. Zhu, P. Lu, C. Ji, X. Wan, Z. Yang, J. Sun *et al.*, Proc. Nat. Acad. Sci. U.S.A. **113**, 2904 (2016).
[40] J. L. Zhang, S. J. Zhang, H. M. Weng, W. Zhang, L. X. Yang, Q. Q. Liu, S. M. Feng, X. C. Wang, R. C. Yu, L. Z. Cao, L. Wang, W. G. Yang, H. Z. Liu, W. Y. Zhao, S. C. Zhang *et al.*, Proc. Nat. Acad. Sci. U.S.A. **108**, 24 (2011).
[41] F. Duan and J. Guojun, *Introduction to Condensed Matter Physics* (World Scientific, Singapore, 2005), Vol. 1 .
[42] B. K. Godwal, A. Jayaraman, S. Meenakshi, R. S. Rao, S. K. Sikka, and V. Vijayakumar, Phys. Rev. B **57**, 773 (1998).
[43] X. Li, J. Sun, P. Shahi, M. Gao, A. H. MacDonald, Y. Uwatoko, T. Xiang, J. B. Goodenough, J. Cheng, and J. Zhou, Proc. Nat. Acad. Sci. U.S.A. **115**, 9935 (2018).
[44] J. A. Sans, F. J. Manjón, A. L. J. Pereira, R. Vilaplana, O. Gomis, A. Segura, A. Muñoz, P. Rodríguez-Hernández, C. Popescu, C. Drasar, and P. Ruleova, Phys. Rev. B **93**, 024110 (2016).
[45] B. Lorenz and C. Chu, in *Frontiers in Superconducting Materials* (Springer, Berlin, 2005), pp. 459–497.
[46] J. Hayashi, I. Shirotani, Y. Tanaka, T. Adachi, O. Shimomura, and T. Kikegawa, Solid State Commun. **114**, 561 (2000).
[47] L. D. Jennings and C. A. Swenson, Phys. Rev. **112**, 31 (1958).
[48] T. Smith and C. Chu, Phys. Rev. **159**, 353 (1967).